Statistical Analysis of Discontinuities in Solar Wind ACE Data and Comparison with Intermittent MHD Turbulence — Source link ↗

Antonella Greco, Antonella Greco, William H. Matthaeus, Sergio Servidio ...+2 more authors

Institutions: University of Calabria, University of Delaware, University of Buenos Aires

Related papers:

- Intermittent MHD structures and classical discontinuities

- Flux tube texture of the solar wind: Strands of the magnetic carpet at 1 AU?

- Identifying intermittency events in the solar wind

- Evidence for Inhomogeneous Heating in the Solar Wind

- Statistical association of discontinuities and reconnection in magnetohydrodynamic turbulence

Share this paper: ⓕ 🐦 in ✉

View more about this paper here: https://typeset.io/papers/statistical-analysis-of-discontinuities-in-solar-wind-ace-3yk2u15ulz

STATISTICAL ANALYSIS OF DISCONTINUITIES IN SOLAR WIND *ACE* DATA AND COMPARISON WITH INTERMITTENT MHD TURBULENCE

A. GRECO[1,2], W. H. MATTHAEUS[2], S. SERVIDIO[2], P. CHUYCHAI[2], AND P. DMITRUK[3]
[1] Dipartimento di Fisica, Universita della Calabria, Rende, Italy
[2] Bartol Research Institute, Department of Physics and Astronomy, University of Delaware, DE, USA
[3] Instituto de Astronomía y Física del Espacio (CONICET-UBA) and Departamento de Física (FCEN-UBA), Buenos Aires, Argentina
Received 2008 July 4; accepted 2008 December 1; published 2009 January 13

ABSTRACT

The comparison between *Advanced Composition Explorer* (*ACE*) solar wind data and simulations of magnetohydrodynamic (MHD) turbulence shows a good agreement in the waiting-time analysis of magnetic field increments. Similarity between classical discontinuity identification and intermittency analysis suggests a dynamical connection between solar wind discontinuities and intermittent MHD turbulence. Probability distribution functions of increments in *ACE* data and in simulations reveal a robust structure consisting of *small random currents*, *current cores*, and intermittent *current sheets*. This adds to evidence that solar wind magnetic structures may emerge fast and locally from MHD turbulence.

Key words: interplanetary medium – MHD – plasmas – solar wind – Sun: magnetic fields – turbulence

1. INTRODUCTION

Simulations of magnetohydrodynamic (MHD) turbulence (Politano et al. 1998; Biskamp & Muller 2000) and solar wind observations (Burlaga 1991; Marsch & Tu 1994; Horbury et al. 1997; Sorriso-Valvo et al. 1999; Burlaga et al. 2006) each show evidence for intermittency in the form of characteristic small-scale structures. A possibly related phenomenon is the well-known frequent appearance of structures traditionally identified as magnetic discontinuities in the solar wind (Burlaga 1968; Tsurutani & Smith 1979) (TS); for a review see Ness & Burlaga (2001). A recent simulation study of Greco et al. (2008) showed that intermittency- and discontinuity-identification methods give similar distributions of events. It is possible therefore that a substantial fraction of the observed discontinuities may be related to *flux tube boundaries* and intermittent structures that appear spontaneously in MHD turbulence (Matthaeus & Montgomery 1980; Matthaeus & Lamkin 1986; Carbone et al. 1990; Veltri 1999; Vasquez et al. 2007; Servidio et al. 2008). An alternative view is that solar wind discontinuities are not representative of turbulence, and convect passively from the source regions of the solar wind (Borovsky 2008). In this Letter, we further examine the link between intermittent turbulence and MHD discontinuities, directly comparing statistical analysis from solar wind data and simulations of MHD turbulence. We employ the *Advanced Composition Explorer* (*ACE*) interplanetary magnetic field data set. We also analyze three-dimensional (3D) compressible Hall MHD (HMHD) simulations (Dmitruk & Matthaeus 2006) and higher spatial resolution two-dimensional (2D) compressible MHD simulations.

We show that the probability density functions of waiting times (WTs) between classical discontinuities identified in the solar wind and in the MHD simulations are essentially the same on inertial scales. Since we have shown in Greco et al. (2008) that MHD turbulence produces intermittent current sheets in sufficient numbers to account for many of the jumps observed at small scales, here we cannot rule out that some of the discontinuities identified in the solar wind are produced by a turbulent MHD cascade.

2. SIMULATIONS AND SOLAR WIND DATA

3D HMHD simulations are carried out using a Fourier pseudo-spectral method, a periodic box of side $2\pi L_0$, and 256^3 spatial grid points. We consider two cases: the first has *plasma beta* $\beta = 1$, *correlation length* $\lambda_c = 2\pi L_0/8$, i.e., small compared to the box size, and large mean field $B_0 = 4$ in the x direction. The second one has larger $\beta = 16$, larger correlation length $\lambda_c = 2\pi L_0/4$, and smaller $B_0 = 1$. For both runs, the *Alfvénic Mach number* is 1, the *magnetic Reynolds number* is $R_m = 1000$, and the dimensionless resistivity and viscosity $= 1/1000$. The magnetic and velocity field modal spectra are flat out to a "bendover scale" $k_{bend} \sim 4$ and $k_{bend} \sim 8$, respectively, at which the initial power spectrum steepens. The initial dissipation wavenumber is $k_{diss} \sim 100$. We report on representative strong turbulence results at $t = 0.5t_A$ (t_A is the Alvfén time), when the energy dissipation is near its peak value.

From simulations, we obtain the magnetic field **B**, the current density **J**, the velocity **v**, and the density ρ. To simulate spacecraft measurements, we interpolate the data along a path through the simulation box. When the trajectory reaches the boundary of the periodic box, the path returns to another side of the box. To avoid spurious periodicity effects, we choose the trajectory at an angle relative to the mean field and the Cartesian axes. Thus, when the trajectory re-enters the box, it is displaced from the initial position by more than a correlation scale. This procedure can continue for a number of re-entries, producing a total trajectory much longer than the box side (Greco et al. 2008).

2D compressible MHD simulations are carried out also in a periodic Cartesian box in (x, y), with mean field B_0 chosen along the out-of-plane z direction. The code uses fourth-order finite difference scheme and the method described by Ghosh et al. (1993). The simulation parameters are chosen to be comparable with the 3D case: $\lambda_c = 2\pi L_0/10$, $B_0 = 4$, $\beta \simeq 4$, and $R_m = 1700$. We include 2D simulation because it allows higher Reynolds number (higher resolution), because it facilitates visualization, and (see below) its statistics may in some ways correspond more closely to solar wind statistics (Sorriso-Valvo et al. 2000).

The available solar wind data set includes 16 s averages of the vector magnetic field from the Magnetic Field Experiment (MAG) on *ACE*. The time interval spanned from day (7:0:0:13 etc) to day 33:23:59:55 during 2001 for a total of 27 days (one Bartels rotation).

3. IDENTIFICATION OF EVENTS

We analyze the time series of the magnitude of magnetic field vector increments (from 3D HMHD simulations and solar wind data) $|\Delta\mathbf{B}| = |\mathbf{B}(s + \Delta s) - \mathbf{B}(s)|$ at points in space separated by Δs, as in standard methods (Tsurutani & Smith 1979). We choose $\Delta s = 2\Delta x = 0.0625\lambda_c$ for the $\beta = 1$ run and the scale $\Delta s = 4\Delta x = 0.0625\lambda_c$ for the $\beta = 16$ run. These separations correspond roughly to the boundary between the dissipation and inertial ranges. Δx is the spatial grid size in the simulations. To compare HMHD simulations with the solar wind data set, we assume that the correlation scale in the solar wind is 1.2×10^6 km (Matthaeus et al. 2005) and that discontinuities convect past the spacecraft at an average speed of $\sim$400 km s^{-1}. The discontinuity identification in the solar wind data was carried out using a time separation of $\Delta t = 4$ min. This is approximately equivalent, under the assumed frozen-in flow condition, to a separation of $\Delta s = 2\Delta x$ and $\Delta s = 4\Delta x$ using $\Delta t = \Delta s/V_{sw}$ and normalizing lengths to λ_c.

Besides the standard statistical measure $|\Delta\mathbf{B}|$, we compute another time series (from both simulations and solar wind data) which is a measure related to intermittency, that is, the normalized partial variance of increments (PVI)

$$\mathfrak{I}^{(2)} = \frac{|\Delta\mathbf{B}|^2}{\Sigma^2}, \qquad (1)$$

where $\Sigma^2 = \sum_i |\Delta\mathbf{B}|_i^2$. PVI is related to the kurtosis of the increments, thus establishing a quantitative connection between large variations of PVI and intermittency. In order to identify intermittent events, we choose a threshold value of PVI. To calibrate the method, we fix a threshold, and all data above this threshold are excluded. Then, we recalculate the kurtosis using the remaining data. This is repeated with varying values of the threshold until the kurtosis of the remaining signal is equal to the value expected for the squared modulus of a random vector having independent Gaussian distributed components. This provides an estimate of the effectiveness of identifying intermittent structures using PVI thresholds.

Following the TS method, we put two thresholds on the $|\Delta\mathbf{B}|$ simulation and solar wind time series. One is that $|\Delta\mathbf{B}|/B_L$ across the discontinuity must exceed $1/2$ where B_L is the larger of the field magnitudes on either side of the discontinuity. The second TS threshold was computed as $|\Delta\mathbf{B}| > 2\delta$, where δ is the level of fluctuations in the vicinity of discontinuity. Using this implementation of the TS method, we compute a series of discontinuities, from the HMHD simulations and the solar wind data set.

We now compare event identification using the TS and PVI methods. First, we compute the probability density function (PDF) of the WT (or distance) between the events in each set of data. The WT measures the elapsed time between the end of an event and the beginning of the next one. Our purpose is to examine if the probability density functions of the WTs support a possible link between the intermittent nature of MHD turbulence structures and solar wind discontinuities.

In Figure 1(a) the comparison between the PDFs of WTs identified by the implementation of TS and PVI methods using
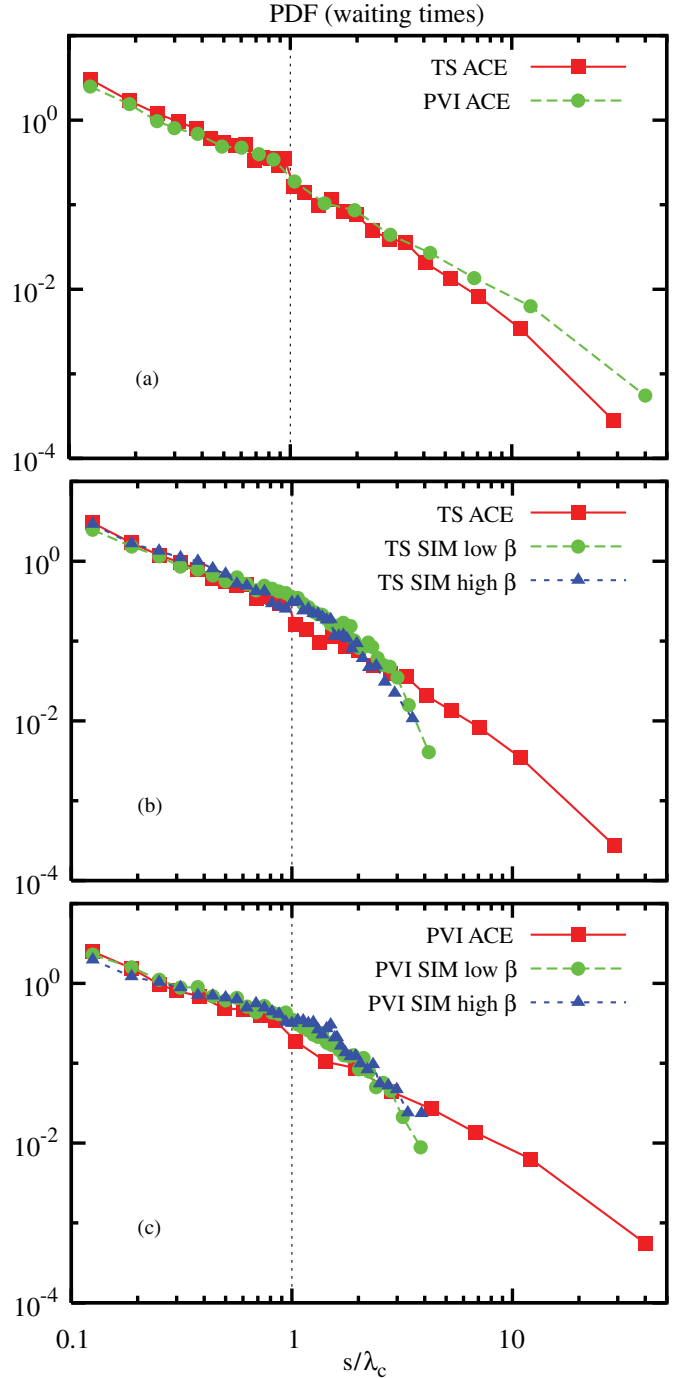

Figure 1. Panel (a): PDFs of WT identified by the implementation of TS and PVI methods using *ACE* data. Panel (b): PDFs of WT identified by the implementation of TS method using *ACE* data and using the two HMHD simulation data set. Panel (c): PDFs of WT identified by the implementation of PVI method using *ACE* data and using two HMHD simulation data set. Waiting distance s is normalized to the correlation length λ_c.

the *ACE* data set is shown. The good agreement suggests that the performance of the two methods is comparable also in the case of solar wind data and not only for the simulation data set as shown in an earlier work of Greco et al. (2008). Many of the events selected by the two methods are the same and the correlation coefficient between PVI and the TS events is 0.74.

In Figure 1(b) three curves are reported: the TS method using *ACE* data and results from the two HMHD simulations (both high and low plasma β). The same, for the PDFs of WTs

identified by the PVI method, is shown in Figure 1(c). Both simulations reproduce the solar wind data quite accurately.

The last two panels have several implications: the two HMHD simulations, even though they are characterized by different values of plasma β, mean magnetic field, and correlation length, can capture the essential statistical features of the frequency of occurrence of solar wind structures or discontinuities. This suggests a sort of universal behavior, particularly since the simulations and solar wind probably have very different (effective) Reynolds numbers. Good agreement is found for scales smaller than around $\sim 1\lambda_c$. Beyond this, departures are not surprising since the large-scale structures in the solar wind are very different from those in the simulations. The box contains only ~ 4–8 correlation lengths, and has no large-scale features other than periodicity. The similarity of the distributions at scales $< \lambda_c$, shown in Figures 1(b) and (c), provides clear evidence that both the discontinuities (b) and the intermittent structures (c) that appear in the simulations have a statistical resemblance to the analogous structures found in the solar wind at these scales. Panel (a) links the two, showing that discontinuities and intermittency may be related. These results support the possible link between the intermittent nature of MHD turbulence and the distribution of solar wind discontinuities.

4. ANALYSIS OF THE STRUCTURE OF THE PDFS

The similarity of the WTs motivates us to look now in further detail at the PDFs of the increments. For inertial range separations the increments are well known (e.g., Marsch & Tu 1994; Sorriso-Valvo et al. 1999) to exhibit departures from a Gaussian distribution, with enhanced probability of large values signifying intermittency (Monin & Yaglom 1975). PDFs have also been studied in simulations (Politano et al. 1998; Biskamp & Muller 2000). Here, we subject both solar wind and simulation data to exactly the same analysis and provide a direct comparison.

For the solar wind case, we divided the original *ACE* magnetic field data into subintervals of 12 hr and normalized the variable $|\Delta\mathbf{B}|$ and its components to the standard deviations within each subinterval (Sorriso-Valvo et al. 1999; Bruno et al. 2001). A separation of $\Delta t = 4$ minutes is employed, as above. For both 3D and 2D simulations the separation Δs is chosen so that $\Delta s/\lambda_c \approx 0.08$. This corresponds to the solar wind case using $\Delta t = 4$ minutes and frozen-in flow at 400 km s^{-1}. At these scales, the signatures of intermittency are expected. In fact, we have examined (not shown here) a range of separations and found that the PDFs make a transition from Gaussian at large scales to non-Gaussian at small scales, fully consistent with standard representations of intermittency in turbulence (Marsch & Tu 1994; Sorriso-Valvo et al. 1999; Burlaga et al. 2003). The bursty fluctuations of the PVI series contribute to the fat tails in the distribution at $\Delta t = 4$ minutes.

In Figure 2, we show PDFs of the z component of the vector $\Delta\mathbf{B}$ for *ACE* data, and for two simulation runs—a 2D MHD run and a 3D HMHD run. The argument of each PDF is normalized in each case by its standard deviation. These PDFs are compared to a unit-variance Gaussian distribution.

The inertial range solar wind PDF has a typical shape with a narrow peak and fat tails (Marsch & Tu 1994). The 3D HMHD simulation PDF presents an interesting comparison to the solar wind case: both are non-Gaussian, but the 3D simulation lies closer to the Gaussian reference curve at all values. The solar wind is more intermittent than the simulation, possibly because the simulation has modest resolution ($\sim$ two decades) relative
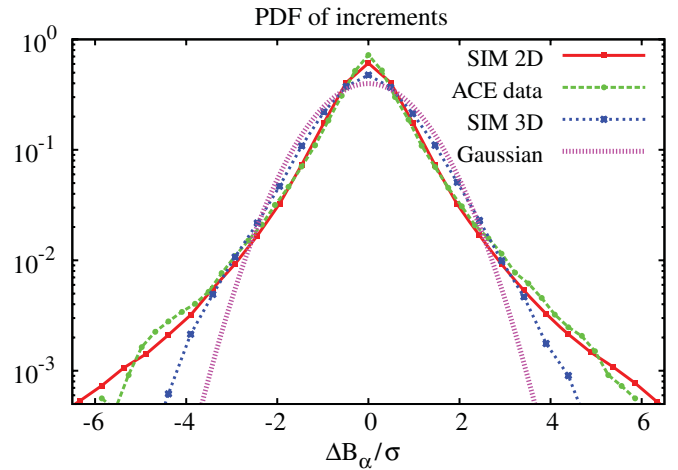

Figure 2. The PDFs of normalized increments designated by $\Delta B_\alpha/\sigma$, where for the *ACE* data this indicates $\Delta B_r/\sigma_{12h}$, the radial magnetic field increment at 4 minutes separation evaluated over 12 hr samples and normalized by the 12 hr standard deviation (green); for the 3D HMHD simulation this becomes $\Delta B_z/\sigma$, increments of a perpendicular component (z) normalized by its standard deviation (blue); for the 2D simulation this becomes the composite PDF of $\Delta B_x/\sigma_x$ and $\Delta B_y/\sigma_y$, the standard-deviation-normalized increments of the two magnetic components perpendicular to the uniform applied magnetic field (red). For comparison a unit variance Gaussian is also shown (pink). The values of the kurtosis are: 14 for the *ACE* data, 10 for the 2D simulation, and 5 for the 3D HMHD simulation.

to the broader-band ($\sim$ three decades) solar wind. That is, the effective Reynolds number is larger in the solar wind case. The 2D MHD simulation lies closer to the solar wind case at all values. This may be due to the higher, approximately three-decade resolution of the 2D case. With higher bandwidth, more singular localized current structures can form, leading to a more non-Gaussian PDF. The better agreement might also be due to spectral anisotropy: the solar wind is "older" and possibly more anisotropic than the 3D simulation, which started with an isotropic initial condition. There has been a frequent suggestion (Bieber et al. 1994, 1996) that the solar wind contains a substantial admixture of highly anisotropic quasi-2D fluctuations.

The solar wind and simulation PDFs (Figure 2) are very similar. Each shows transition from sub-Gaussian to super-Gaussian behavior at almost the same values of its argument. These transitions occur at about $\pm 1\sigma$ and near $\pm 3\sigma$. At values with the band $|\Delta B_\alpha| < 1\sigma$ (see Figure 2) all the three PDFs are super-Gaussian. In the bands defined by $1\sigma < |\Delta B_\alpha| < 3\sigma$, all the three PDFs are sub-Gaussian. At larger values $|\Delta B_\alpha| > 3\sigma$ all the three PDFs are super-Gaussian—these are the fat tails that are a familiar signature of intermittency.

Finally, we examine the 2D simulation to identify which kind of structure contributes within each of these three bands, designated as regions I, II, and III. Figure 3 shows the PDFs of the out-of-plane electric current density J_z relative to the reference Gaussian. This PDF is almost a precise match for the PDF of 2D inertial range increments in Figure 2. Now we numerically select points that contribute to each band, and produce an image consisting of those points. We superpose this image with a plot of magnetic field lines in the x–y plane. The results for regions I, II, and III are shown separately in Figure 3. A physically appealing interpretation emerges: region I consists of very low values of fluctuations that lie mainly in the lanes between magnetic islands. Region II consists of sub-Gaussian current cores that populate the central regions
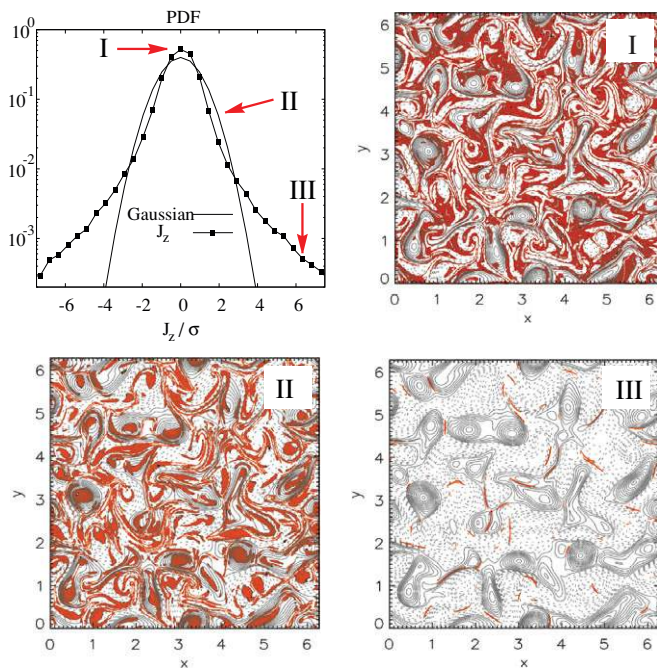
Figure 3. PDF of the out-of-plane electric current density J_z from the 2D simulation, compared to a reference Gaussian (standard deviation σ). For each region I, II, and III, magnetic field lines (contours of constant magnetic potential A_z: > 0 solid, < 0 dashed) are shown; the colored (red) regions are places where the selected band (I, II, or III) contributes.

of the magnetic islands (or flux tubes). Region III is composed of the coherent small-scale current sheet-like structures that form the sharp boundaries between the magnetic flux tubes.

The current sheets in region III represent the well-known small-scale coherent structures of MHD turbulence (Matthaeus & Montgomery 1980; Veltri 1999; Servidio et al. 2008), that are linked to the magnetic field intermittency. The current cores in region II are required by Ampère's law, for any flux tube carrying nonzero current. The size and poloidal flux profiles of these tubes can in principle be related to the sub-Gaussian shape of the increment PDF in this region. Finally, region I consists of local wave-like (low nonlinearity) activity and other transient random currents. These are not associated with small-scale localized phase-coherence, and lie in the magnetic separatrix regions. Region I is formally super-Gaussian, but its shape is roughly parabolic, and would probably lie close to a Gaussian if the standard deviation was not dominated by region III. This classification provides a real-space picture of the nature of intermittent MHD turbulence.

5. CONCLUSIONS

We computed WT distributions of events, defined as large changes in the magnitude of the magnetic field vector at separations lying in the power-law inertial range, for simulations and for solar wind data. Methods similar to those used in the identification of classical MHD discontinuities were employed, along with methods based on intermittency analysis. Previously, the most common idea has been that these structures can be identified as ideal MHD discontinuities. Here, we are not examining the normal magnetic field which is required to distinguish between tangential and rotational discontinuities

(Neugebauer 2006). Using our approach, the intermittency and discontinuity methods behave similarly, and the solar wind magnetic field and MHD simulation analysis are in close agreement for scales comparable to and smaller than the correlation scale. Direct comparison of the probability distributions of increments at inertial range separations in the MHD simulations and in the solar wind magnetic field reveals a very similar three-part functional form. For the 2D case, these are identified as super-Gaussian current sheets, sub-Gaussian flux tube cores, and weak sub-Gaussian currents between flux tubes. These results are consistent with the hypothesis that solar wind intermittency and many or most of its discontinuities are produced by MHD turbulence, even if we have not ruled out that some of these features originate in the lower corona. It is possible that many or even most of the current structures in the solar wind, particularly inertial range structures that contribute to the tails of the PDFs of increments of **B**, are formed in situ by local rapid relaxation processes associated with turbulence (Servidio et al. 2008).

REFERENCES

Bieber, J. W., Matthaeus, W. H., Smith, C. W., Wanner, W., Kallenrode, M.-B., & Wibberenz, G. 1994, ApJ, 420, 294
Bieber, J. W., Wanner, W., & Matthaeus, W. H. 1996, J. Geophys. Res., 101, 2511
Biskamp, D., & Muller, W.-C. 2000, Phys. Plasmas, 7, 4889
Borovsky, J. E. 2008, J. Geophys. Res., 113, A08110
Bruno, R., Carbone, V., Veltri, P., Pietropaolo, E., & Bavassano, B. 2001, Plan. Space Sci., 49, 1201
Burlaga, L. F. 1968, Sol. Phys., 4, 67
Burlaga, L. F. 1991, J. Geophys. Res., 96, 5847
Burlaga, L. F., Ness, N. F., & Acuña, M. H. 2006, J. Geophys. Res., 111, A09112
Burlaga, L. F., Wang, C., Richardson, J. D., & Ness, N. F. 2006, ApJ, 585, 1158
Carbone, V., Veltri, P., & Mangeney, A. 1990, Phys. Fluids A, 2, 1487
Dmitruk, P., & Matthaeus, W. H. 2006, Phys. Plasmas, 13, 2307
Ghosh, S., Hossain, M., & Matthaeus, W. H. 1993, Comput. Phys. Commun., 74, 18
Greco, A., Chuychai, P., Matthaeus, W. H., Servidio, S., & Dmitruk, P. 2008, Geophys. Res. Lett., 35, L19111
Horbury, T. A., Balogh, A., Forsyth, R. J., & Smith, E. J. 1997, Adv. Space Phys., 19, 847
Marsch, E., & Tu, C. Y. 1994, Ann. Geophys., 12, 1127
Matthaeus, W. H., Dasso, S., Weygand, J. M., Milano, L. J., Smith, C. W., & Kivelson, M. G. 2005, Phys. Rev. Lett., 95, 231101
Matthaeus, W. H., & Lamkin, S. L. 1986, Phys. Fluids, 29, 2513
Matthaeus, W. H., & Montgomery, D. 1980, Ann. N. Y. Acad. Sci., 357, 203
Monin, A. S., & Yaglom, A. M. 1975, Statistical Fluid Mechanics (Cambridge, MA: MIT Press), 2
Ness, N. F., & Burlaga, L. F. 2001, J. Geophys. Res., 106, 15803
Neugebauer, M. 2006, J. Geophys. Res., 111, A04103
Politano, H., Pouquet, A., & Carbone, V. 1998, Europhys. Lett., 43, 516
Servidio, S., Matthaeus, W. H., & Dmitruk, P. 2008, Phys. Rev. Lett., 100, 095005
Sorriso-Valvo, L., Carbone, V., Veltri, P., Consolini, G., & Bruno, R. 1999, Geophys. Res. Lett., 26, 1801
Sorriso-Valvo, L., Carbone, V., Veltri, P., Politano, H., & Pouquet, A. 2000, Europhys. Lett., 51, 520
Tsurutani, B. T., & Smith, E. J. 1979, J. Geophys. Res., 84, 2773
Vasquez, B. J., Abramenko, V. I., Haggerty, D. K., & Smith, C. W. 2007, J. Geophys. Res. (Space Phys.), 112, 11102
Veltri, P. 1999, Plasma Phys. Contr. Fusion, 41, 787